

Numerical Modelling of the Microcavity OPO

D. M. Whittaker

Department of Physics, University of Sheffield, S3 7RH, Sheffield, United Kingdom

A detailed description is provided of a numerical model of the microcavity optical parametric oscillator (OPO). The model is solved on a two dimensional grid, in the time domain, using an alternating-direction implicit method. Results are presented for a system pumped with a gaussian spatial profile beam. It is shown that at high pump powers the OPO signal forms a ring, with low emission at the centre where the pumping is strongest.

To be published in *Physica Status Solidi* (c)

I. INTRODUCTION

The polariton physics in a strongly-coupled semiconductor microcavity includes interesting non-linear optical effects. When resonantly pumped with an off-axis laser, optical parametric oscillator (OPO) behaviour can be obtained, with the spontaneous appearance of signal and idler emission^{1,2}. Since the excitonic non-linearity is $\chi^{(3)}$, the phase matching condition requires $2\omega_p = \omega_s + \omega_i$ and $2k_p = k_s + k_i$, which means that the pump, signal and idler can all be close to resonance with the polariton dispersion. This behaviour has been investigated theoretically by a number of authors, using analytic^{3,4} and numerical⁵ models. However, all these models differ from the experimental setup by assuming that the pump is a plane wave, with uniform excitation of the system, and uniform polariton fields. While such treatments provide useful insights into the OPO, a fuller understanding of the observed behaviour requires a theory which takes into account the finite excitation spot used in experiments. The purpose of this paper is to describe a numerical treatment of a two dimensional microcavity polariton system pumped with a Gaussian beam, solved in the time domain on a discrete spatial grid.

II. THE NUMERICAL MODEL

The model for the OPO is based on the non-linear optics treatment of Ref.⁴. It consists of coupled two-dimensional cavity and exciton fields, ϕ_C and ϕ_X , with a local $\chi^{(3)}$ non-linearity in the exciton to represent the effects of short-range interaction. Both fields have dispersions, described by effective masses M_C and M_X , and are damped with widths γ_C and γ_X . The coupling is characterised by Ω , the Rabi splitting, and Δ , the detuning at normal incidence. The cavity field is driven by a spatially dependent external pump field $f_p(r) \exp(i\omega_p t)$. The time evolution of the fields is thus determined by

$$i \frac{\partial \phi_C}{\partial t} = \left(-\frac{1}{2M_C} \nabla^2 - i\gamma_C + \Delta \right) \phi_C + \frac{1}{2} \Omega \phi_X + f_p(r) \exp(i\omega_p t) \quad (1)$$

$$i \frac{\partial \phi_X}{\partial t} = \left(-\frac{1}{2M_X} \nabla^2 - i\gamma_X + \kappa |\phi_X|^2 \right) \phi_X + \frac{1}{2} \Omega \phi_C \quad (2)$$

To be exact, the form for the $\chi^{(3)}$ nonlinearity should be $\kappa \phi_X^3$. However, for a numerical treatment, it is better to chose $\kappa |\phi_X|^2 \phi_X$, as this is independent of the origin of energy, which can thus be shifted to the exciton frequency. The modified form correctly gives the scattering effects of interest here, but does not describe frequency multiplying effects, which would require extremely small time-steps in the numerics.

For the numerical treatment, this model is discretized on a two dimensional grid, with the differential operators are replaced by hopping terms. The solution is obtained in the time domain, as an initial value problem, using the Crank-Nicholson method⁶. This leads to a semi-implicit time-step formula of the form

$$\left(1 + \frac{1}{2} i H \delta t \right) \psi_{ij}^{n+1} = \left(1 - \frac{1}{2} i H \delta t \right) \psi_{ij}^n, \quad (3)$$

where the vector $\psi_{ij}^n = (\phi_C, \phi_X)^T$ describes the cavity photon and exciton amplitudes on the site (ij) at time-step n . The precise form of the matrix operator H will be specified below.

The problem with solving Eq.(3) in two dimensions is that H is a large matrix (size $N^2 \times N^2$, where N is the length of the edge of the grid), whose structure does not lend itself to efficient numerical solution: there are non-zero terms far from the diagonals. It is better to use an operator-splitting treatment, the alternating direction implicit method⁷,

writing $H = H_x + H_y$, where H_x and H_y respectively contain only x and y hopping terms. Then, each time-step is divided into two sub-steps: first,

$$(1 + \frac{1}{2}iH_x\delta t) \psi_{i(j)}^{n+\frac{1}{2}} = (1 - \frac{1}{2}iH_x\delta t) \psi_{i(j)}^n \quad (4)$$

is solved for every j , then

$$(1 + \frac{1}{2}iH_y\delta t) \psi_{(i)j}^{n+1} = (1 - \frac{1}{2}iH_y\delta t) \psi_{(i)j}^{n+\frac{1}{2}} \quad (5)$$

for every i . Each of these one dimensional strip problems is independent, so it is necessary to solve only $2N$ ($N \times N$) sets of equations. Moreover the matrices H_x and H_y contain non-zero terms only on the diagonal and first three sub-diagonals, which permits a very efficient solution by factorisation⁸.

The part of H_x involving coupling to site i is

$$H_x = \begin{pmatrix} 0 & H^{\text{hop}} & \frac{1}{2}H_{i-1}^{\text{site}} & H^{\text{hop}} & 0 & \dots & \dots \\ \dots & 0 & H^{\text{hop}} & \frac{1}{2}H_i^{\text{site}} & H^{\text{hop}} & 0 & \dots \\ \dots & \dots & 0 & H^{\text{hop}} & \frac{1}{2}H_{i+1}^{\text{site}} & H^{\text{hop}} & 0 \end{pmatrix} \quad (6)$$

where each H is a 2×2 matrix:

$$H^{\text{hop}} = \begin{pmatrix} -t_c^x & 0 \\ 0 & -t_x^x \end{pmatrix} \quad H^{\text{site}} = \begin{pmatrix} 2t_c^x - i\gamma_c + \Delta & \frac{1}{2}\Omega \\ \frac{1}{2}\Omega & 2t_x^x - i\gamma_x + \kappa|\phi_x|^2 \end{pmatrix}. \quad (7)$$

The hopping terms are $t_c^x = (2M_c\delta_x^2)^{-1}$ and $t_x^x = (2M_x\delta_x^2)^{-1}$, with δ_x the x -direction grid spacing. The value of ϕ_x used in the non-linear term is the old value at that site, ie from the right hand side of Eq.(4) or Eq.(5). H_y has a similar form, except δ_y replaces δ_x , though in practice an isotropic grid is used. The factors of $\frac{1}{2}$ multiplying H^{site} are needed to avoid over-counting, because they occur in both H_x and H_y .

Eq.(4), and similarly Eq.(5), is most efficiently solved in two stages: first an intermediate variable ψ^t is calculated using

$$\frac{1}{2}(1 + \frac{1}{2}iH_x\delta t) \psi^t = \psi^n, \quad (8)$$

then it is straightforward to show that $\psi^{n+\frac{1}{2}} = \psi^t - \psi^n$.

To incorporate periodic boundary conditions, Eq.(6) has to be modified by adding hopping terms in the off-diagonal corners of the matrix, coupling the sites at either end of a strip:

$$H_x^p = \begin{pmatrix} & & \dots & 0 & H^{\text{hop}} \\ & & \dots & 0 & 0 \\ \vdots & \vdots & & \vdots & \vdots \\ 0 & 0 & \dots & & \\ H^{\text{hop}} & 0 & \dots & & \end{pmatrix}. \quad (9)$$

Adding these terms breaks the useful diagonal form of the matrix, so a direct solution of Eq.(9) would be inefficient. However, as there are just four extra non-zero entries, the problem can be handled at little numerical cost using the Woodbury formula⁹ to incorporate the extra terms. H_x^p is written as

$$H_x^p = H_x' + \sum_{k=1,2} u_k \otimes v_k \quad (10)$$

where the u_k and v_k are chosen to generate the end hopping terms. An efficient choice is

$$u_1 = (\beta_1, 0, \dots, -t_c^x, 0)^T \quad (11)$$

$$v_1 = (1, 0, \dots, -t_c^x/\beta_1, 0)^T \quad (12)$$

$$u_2 = (0, \beta_2, \dots, 0, -t_x^x)^T \quad (13)$$

$$v_2 = (0, 1, \dots, 0, -t_x^x/\beta_2)^T \quad (14)$$

where $-\beta_1$ and $-\beta_2$ are the first two elements along the main diagonal of H_x . H_x' is a slightly modified version of H_x : the $u \otimes v$ terms produce, as well as the required hopping terms, four additional elements along the main diagonal which have to be subtracted from H_x to obtain the correct H_x^p .

Evaluating the Woodbury formula requires additional solutions of Eq.(8) with u_1 and u_2 on the right hand side, but this is very inexpensive once the factorisation of H_x' is obtained. Hence adding periodic boundary conditions makes little difference to the numerical costs.

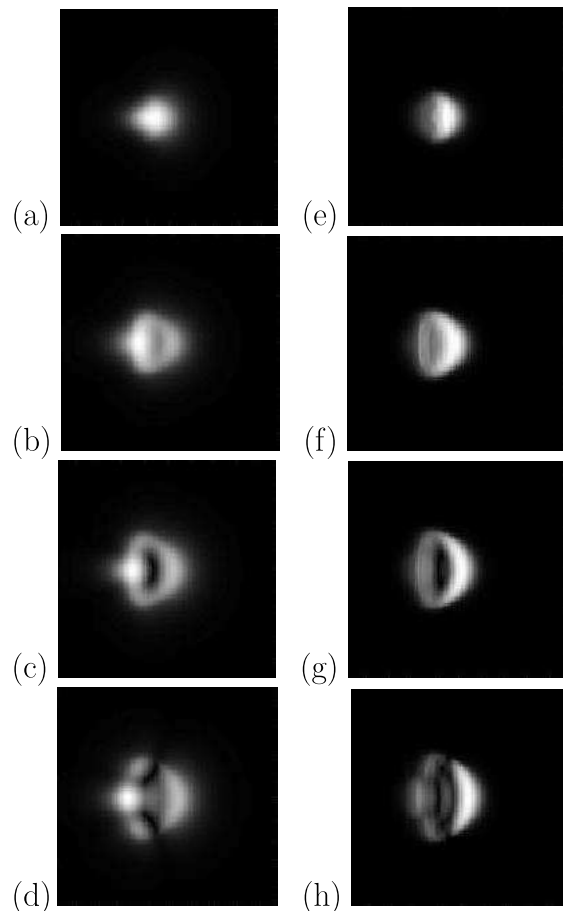


FIG. 1: Grey-scale plots of the OPO states for Gaussian pump beam at 16° with various powers. (a) and (e) are the signal and idler intensities for a peak power of 0.2, just above threshold. The following rows represent pump powers of 0.3, 0.4 and 0.5, with the signal states on the left, the idlers on the right. The lengths of the edges of the squares are $51.2\mu\text{m}$, and the FWHM of the pump beam is $17.05\mu\text{m}$.

III. RESULTS

The results described in this section are for a microcavity with physical parameters typical of a good GaAs structure: the Rabi splitting, $\Omega = 5$ meV, and the line-widths of the exciton and cavity mode are $\gamma_x = \gamma_c = 0.25$ meV. The structure is on-resonance at normal incidence ($k = 0$), and pumped at 16° with a Gaussian beam whose FWHM is $17.05\mu\text{m}$. The cavity mode effective mass is taken to be $3 \times 10^{-5}m_e$, and the exciton mass $0.5m_e$. The spatial grid consists of $(2^7 \times 2^7)$ points with a separation of $0.4\mu\text{m}$, and the time step is 12 fs.

The calculation is started with the fields set to zero, and the solution is then propagated until a steady state is reached, typically after about 10^4 time steps or ~ 100 ps. The pump, signal and idler are then separated by storing the data for a series of time steps, Fourier transforming to the frequency domain, and applying band-pass filters. This process can be carried out in a continuous way using a rolling time window, which allows the observation of dynamical effects occurring on time-scales slow compared to the inverse of the mode separation.

The calculated images show the spatial dependence of the steady-state cavity field intensities in the signal and idler modes at various pump powers. It should be noted that they represent the internal cavity field, which cannot be directly observed experimentally. The emitted light will undergo some additional spatial filtering due to the small k -width of the polariton branches.

Fig.1 shows the calculated signal and idler images for the steady state at various pump powers above threshold. Close to threshold, (a) and (e), only a small spot near to the centre of the image is bright. This is easily understood: for a Gaussian beam profile, the threshold will be reached first where the pump is strongest. At higher pump powers, the emission spot expands, but, instead of the centre becoming brighter, the spot turns into a ring with low intensity in the middle. It can be explained qualitatively using an analytic plane-wave model where the contributions of the

signal and idler to the polariton blue-shifts are taken into account¹⁰. The shifts cause the OPO to switch off above a certain power, which depends on the incidence angle and detuning of the pump beam. This happens first at the centre of the spot, leading to the dark middle. In a Gaussian beam, there will always be a region where the pump power is the range to allow the OPO, so an expanding emission ring should be expected as the power is increased above threshold.

Of course, the strong spatial dispersion of the polariton means that a such a simple picture, relating the OPO intensity to the local value of the pump, is not completely accurate, but it seems to give a reasonable guide. The dispersion effects are responsible for the fact that the ring is not perfectly symmetrical, and breaks up significantly at higher pump powers. However, a bilateral symmetry is always maintained, defined by the incidence plane, which cuts the figure along the x -axis.

Finally, at higher powers than those shown in the Fig.1, the numerics predict that a steady state may not be reached. Instead, the signal and idler undergo a periodic oscillation, maintaining the general ring shape, but with the maximum intensity moving from side to side.

IV. SUMMARY

It has been shown that a full understanding of the microcavity OPO requires a two-dimensional treatment of the spatial structure of the pump beam and the polariton fields. A numerical model describing the spatial and temporal evolution of the system has been derived, and used to predict that the emission spot should form a ring at high pump powers. These results demonstrate that experimental measurements without spatial resolution provide only a limited picture of the OPO behaviour.

-
- ¹ R. M. Stevenson, V. N. Astratov, M. S. Skolnick, D. M. Whittaker, M. Emam-Ismael, A. I. Tartakovskii, P. G. Savvidis, J. J. Baumberg and J. S. Roberts, *Phys. Rev. Lett.* **85** 3680 (2000).
² J. J. Baumberg, P. G. Savvidis, R. M. Stevenson, A. I. Tartakovskii, M. S. Skolnick, D. M. Whittaker and J. S. Roberts *Phys. Rev.* **B62** R16247 (2000).
³ C. Ciuti, P. Schwendimann, B. Deveaud and A. Quattropani, *Phys. Rev.* **B62**, R4825 (2000).
⁴ D. M. Whittaker, *Phys. Rev.* **B63** 193305 (2001).
⁵ N. A. Gippius, S. G. Tikhodeev, V. D. Kulakovskii, D. N. Krizhanovskii and A. A. Tartakovskii, *cond-mat/0312214* (2003); V. D. Kulakovskii, D. N. Krizhanovskii, A. A. Tartakovskii, N. A. Gippius and S. G. Tikhodeev, *Uspekhi Fiz. Nauk* **173**, 995 (2003).
⁶ W. H. Press, B. P. Flannery, S. A. Teukolsky and W. T. Vetterling, *Numerical Recipes (Fortran Version)*, Cambridge University Press (1989), pp.635-642.
⁷ W. H. Press *et al.*, *ibid*, pp. 660-667.
⁸ The linear algebra routines used were from LAPACK; CGBFA, to perform the factorisation, and CGBSL for the back-substitution. See www.netlib.org.
⁹ W. H. Press *et al.*, *ibid*, pp. 66-70.
¹⁰ D. M. Whittaker, *cond-mat/0408286* (2004).